Biochemistry **2003,** *42,* 7769−7779

The Three-Dimensional Structure of Bovine Calcium Ion-Bound Osteocalcin Using ^{1}H NMR Spectroscopy[†]

T. L. Dowd,*[,‡] J. F. Rosen,[‡] L. Li,[§] and C. M. Gundberg[||]

Department of Pediatrics, Montefiore Medical Center, Albert Einstein College of Medicine, Bronx, New York, The National Institute of Environmental Health Sciences, Research Triangle Park, North Caroline, and Department of Orthopedics, Yale University School of Medicine, New Haven, Connecticut

Received March 24, 2003; Revised Manuscript Received May 5, 2003

ABSTRACT: Structural information on osteocalcin or other noncollagenous bone proteins is very limited. We have solved the three-dimensional structure of calcium bound osteocalcin using ^{1}H 2D NMR techniques and proposed a mechanism for mineral binding. The protons in the 49 amino acid sequence were assigned using standard two-dimensional homonuclear NMR experiments. Distance constraints, dihedral angle constraints, hydrogen bonds, and ^{1}H and ^{13}C chemical shifts were all used to calculate a family of 13 structures. The tertiary structure of the protein consisted of an unstructured N terminus and a C-terminal loop (residues 16−49) formed by long-range hydrophobic interactions. Elements of secondary structure within residues 16−49 include type III turns (residues 20−25) and two α-helical regions (residues 27−35 and 41−44). The three Gla residues project from the same face of the helical turns and are surface exposed. The genetic algorithm−molecular dynamics simulation approach was used to place three calcium atoms on the NMR-derived structure. One calcium atom was coordinated by three side chain oxygen atoms, two from Asp30, and one from Gla24. The second calcium atom was coordinated to four oxygen atoms, two from the side chain in Gla 24, and two from the side chain of Gla 21. The third calcium atom was coordinated to two oxygen atoms of the side chain of Gla17. The best correlation of the distances between the uncoordinated Gla oxygen atoms is with the intercalcium distance of 9.43 Å in hydroxyapatite. The structure may provide further insight into the function of osteocalcin.

The family of vitamin K-dependent γ-carboxylated calcium binding proteins is important in a variety of tissues and cellular functions. The formation of γ-carboxyglutamic acid (Gla)[1] in the liver derived blood clotting factors, for example, results in calcium-dependent conformational changes in the proteins and functionally important interactions with acidic phospholipid surfaces (*1*−*3*). The predominant Gla protein found in bone matrix is osteocalcin (*4*, *5*), a small Ca^{2+} binding protein containing three Gla residues which are thought to facilitate the protein's adsorption to hydroxyapatite (*6*). Because of its unique calcium binding properties, early functional studies suggested that osteocalcin controlled the nucleation or deposition of mineral in bone (*7*−*10*). However, more recent evidence indicates that osteocalcin is not related to events which allow mineral deposition to occur but, rather, that it participates in regulation of mineralization or bone turnover. For example, several studies have suggested that osteocalcin functions as a matrix signal for resorption through the recruitment and differentiation of bone resorbing cells (*11*−*15*). On the other hand, the osteocalcin knock-out mouse has been shown to have an increased bone mass and increased bone formation rates, implying that osteocalcin may function to limit bone formation (*16*). Further studies on the knock-out mouse also suggest a role for osteocalcin in mineral maturation and bone remodeling (*17*).

Despite the increase in functional knowledge, structural information on the protein is limited. In all species examined, the central portion of the molecule is strongly conserved (*18*). This region includes a disulfide loop (Cys23−Cys29) and three γ-carboxyglutamic acid residues (Gla) at positions 17, 21, and 24. Circular dichroism (CD) and ^{1}H NMR studies show that the apo-protein is in a random coil conformation while the addition of millimolar levels of Ca^{2+} induces an α-helical conformation in the molecule (*19*−*23*).

Empirical modeling predicts two antiparallel α-helical domains, several β-turns, and a β-sheet structure resulting in an accessible COOH terminus (*19*). In this model, spatial projections of the side chains of the three Gla residues coincide with the spacing between the Ca^{2+} atoms in the hydroxyapatite crystal (*24*) allowing for binding to the bone via uncoordinated Gla carboxyl groups.

At present there is no high-resolution structure of osteocalcin nor of any noncollagenous bone protein. This is in sharp contrast to other calcium binding proteins such as

[†] Support for this project was provided by NIH Grant ES-02030 to T.D., support from the Division of Environmental Sciences, Children's Hospital at Montefiore (CHAM), at the Albert Einstein College of Medicine to T.D., and NIH Grant AR-38460 to C.G.

* Corresponding author. Address: Montefiore Medical Center, Moses Bldg. Rm. 401, 111 East 210th Street, Bronx, NY, 10467. Phone: 718-920-2276. Fax: 718-920-4377. E-mail: dowd@aecom.yu.edu.

[‡] Albert Einstein College of Medicine.

[§] The National Institute of Environmental Health Sciences.

[||] Yale University School of Medicine.

[1] Abbreviations: Gla, γ-carboxyglutamic acid; Fmoc, 9-flourenylmethyloxycarbonyl; CD, circular dichroism; NMR, nuclear magnetic resonance; HSQC, heteronuclear single-quantum correlation; NOE, nuclear Overhauser effect; NOESY, NOE spectroscopy; rmsd, root-mean-square deviation; TOCSY, total correlation spectroscopy.

10.1021/bi034470s CCC: $25.00
Published on Web 06/06/2003

calmodulin (*25*, *26*), troponin C (*27*, *28*), and calbindin (*29*) or other Gla-containing proteins (*1*−*3*). A high-resolution structure of Ca^{2+}-osteocalcin will provide information on a new class of proteins. It may also shed light on the function of the protein and its interaction with bone mineral at the molecular level. The purpose of this study is to determine the high-resolution 3D structure of bovine Ca^{2+}-osteocalcin using 2D ^{1}H NMR techniques.

EXPERIMENTAL PROCEDURES

Sample Preparation. Osteocalcin was purified from bovine bone powder as previously described (*30*). The purity of the protein was determined by PAGE, reverse-phase HPLC, and amino acid analysis and further characterized by electrospray mass spectrometry.

Some of the bovine osteocalcin in this study was also synthesized using solid-phase peptide synthesis methodology on an ABI 433 peptide synthesizer using Fmoc protocols as previously described (*22*, *31*).The disulfide bond between the two Cys residues was formed by slow air oxidation methods (*32*), and the protein was purified by reverse-phase HPLC. Synthetic bovine osteocalcin was characterized by analytical HPLC, electrospray mass spectrometry, and amino acid analysis. The synthetic protein was found to give similar CD, 1D, and 2D NMR spectra and to bind to hydroxyapatite in a manner similar to the osteocalcin prepared from calf bone. Some of the 2D experimental data were also collected on the synthetic osteocalcin.

Protein solutions were titrated with $CaCl_2$ to determine the amount of total Ca^{2+} needed to obtain the maximum conformational change. Solutions for NMR spectroscopy performed on H_2O samples contained 1.3−1.6 mM protein, 6 mM $CaCl_2$, 20 mM NaCl, and 10% ^2H_2O at a pH of 6.8 at 37, 27, and 22 °C. For samples collected in ^2H_2O, the sample was lyophilized from ^2H_2O several times and then resuspended in 99.96% ^2H_2O. The pH was adjusted before each experimental run, and measurements after the experiment was completed found the pH was unchanged and stable.

Analytical Ultracentrifugation. Sedimentation equilibrium experiments were performed on apo- and Ca^{2+}-bound osteocalcin in order to determine the oligomerization state of the protein. The absorption optics of a Beckman Optima XL-I analytical ultracentrifuge running an AN-50Ti rotor were used to measure the protein concentration gradient at 280 nm in buffer containing 20 mM NaCl at 37 °C and pH 6.8 with and without 6 mM $CaCl_2$. For each condition, data were collected at three concentrations (24, 64, and 94 μM) and two rotor speeds (29 000 rpm and 38 000 rpm). Protein concentration was determined using an extinction coefficient at 280 nm of $A^{1\%}{}_{1cm} = 13.3$. Absorbance scans at 280 nm were taken after 22 and 24 h at speed. Equilibrium was assumed to have been reached if the scans were identical. Typically two scans were taken at 24 h at each rotor speed.

Data analysis was performed using the Beckman XL-A/XL-I data analysis software package within Microcal, ORIGIN v4 using values of the buffer density and protein partial specific volume determined as described below. Each analysis consists of the six absorbance scans taken of the three initial proteins concentrations at each of the two rotor speeds. Buffer densities (0.994 g/mL) were determined using a Mettler DE40 density meter operated at the experimental temperature, as well as in the program Sednterp v1.03 (*33*). The partial specific volume (0.7334 mL/g) was determined from amino acid residue composition and calculated in Sednterp.

NMR Spectroscopy. All NMR spectra were collected on a Bruker DRX 600 MHz spectrometer. The double gradient echo method of Hwang and Shaka (*34*) was used for water suppression in all 2D experiments. All 2D data sets in H_2O were collected at 310, 300, and 295 K to aid in assignment by removing overlap and for observation of α protons near the H_2O resonance. Either TPPI or States-TPPI was used for quadrature detection in the second dimension (*35*, *36*). The data were processed using NMRPipe (*37*) and extended using linear prediction and zero filling. The data were analyzed using NMRView (*38*).

All proton resonances were assigned using standard procedures developed by Wüthrich (*39*). Intraresidue proton resonance assignments were made using DQF-COSY and both short (17 ms) and long (60 ms) mixing time TOCSY experiments using 640 t1 increments (*40*). A natural abundance ^{13}C−H HSQC experiment was collected with 160 t1 increments to obtain C_α and C_β chemical shifts. Sequential assignments and distance constraints were obtained from NOESY spectra collected using a 150 ms mixing time and 640 t1 increments. TOCSY and NOESY spectra were also collected in ^2H_2O to obtain spin system assignments close to the H_2O resonance as well as to distinguish between aromatic and amide protons.

Structure Calculation. NOE cross-peak intensities were classified as strong, medium, and weak and were converted to distance restraints of 1.8−2.8, 1.8−3.4, and 1.8−5.5 Å, respectively. Atoms that were not stereospecifically assigned were treated as pseudoatoms and given correction distances according to procedures in Wüthrich (*39*). Dihedral angle restraints were obtained from H_α, $^{13}C_\alpha$, and $^{13}C_\beta$ chemical shift analysis using the program Talos (*41*). Ranges for the side chain χ_1 and χ_2 torsion angles were determined by the program HABAS within DYANA, which yields constraints which are compatible with all local NOE distance constraints (*42*). Amide proton temperature coefficients were calculated from the proton chemical shift change from 15 to 37 °C. Any amide proton which shifted less than 5.5 ppb/K was considered likely to be hydrogen bonded. Initial structures were calculated using NOE constraints, dihedral angle constraints, and H_α and $^{13}C_\alpha$, chemical shifts by simulated annealing, and torsional angle dynamics as applied in the program CNS (*43*). A hydrogen bond analysis was performed on all structures using the program MolMol (*44*). A hydrogen bond was considered to occur if it was present in greater than 60% of the structures and if the donor proton had a reduced temperature coefficient. Final structures were then calculated using CNS with hydrogen bonds as additional constraints. The 13 lowest-energy structures were evaluated with AQUA and PROCHECK-NMR (*45*).

Identification of the Positions of Ca^{2+} Ions in Osteocalcin. The previously described genetic algorithm-molecular dynamics method (*46*) was used to place the calcium atoms in osteocalcin and also used for further energy minimization and refinement of the metal-bound structure. The initial structures used were the 13 best conformers determined by NMR of the Ca^{2+}−osteocalcin complex. The genetic algorithm was used to determine potential calcium binding sites

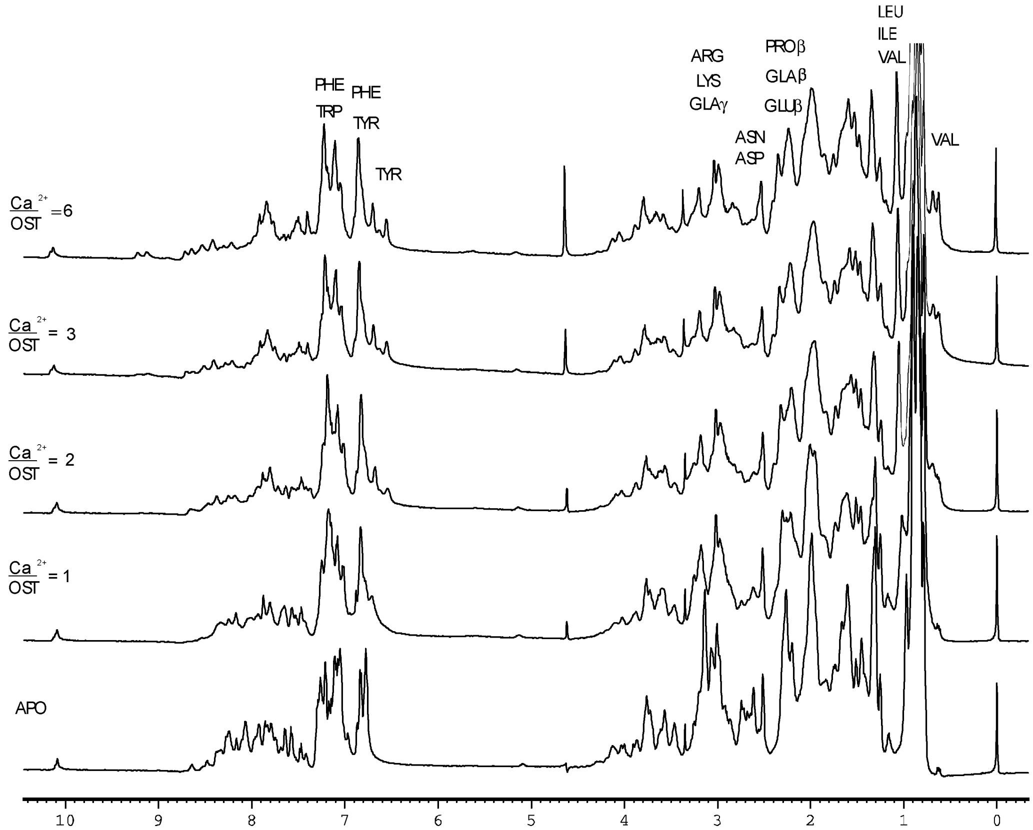

FIGURE 1: ^{1}H 1D NMR spectra of osteocalcin titrated with $CaCl_2$. The solution contained 1.0 mM osteocalcin, 20 mM NaCl, and 10% ^2H_2O at a pH of 6.8 and was collected at 37 °C. The Ca^{2+}/Ost ratios are shown to the left of each spectrum. The signal at 4.6 ppm is from the H_2O protons.

by searching all O−O midpoints which were within 7 Å of each other. There were approximately 300 such midpoints in each of the 13 conformers. The genetic algorithm (*46*) was subsequently used to search for three Ca^{2+} binding sites on each conformer. Multiple independent runs of searches were carried out for each conformer and the sites with the lowest potential energy, determined within the program Amber (*47*), were taken as the sites for the conformer. The energies were converged (the same lowest-energy between runs). Among the 13 conformers, the most frequently occurring sites all had three Gla residues coordinating the three Ca^{2+} in a similar fashion. This result suggests that it is reasonable to average the 13 initial NMR structures and apply the genetic algorithm on the average structure. The average structure and the predicted Ca^{2+} sites were further refined using a molecular dynamics simulation with Particle-Mesh Ewald (*48*) to accommodate long-range electrostatics and determine the best positions of the calcium coordinating residue side chains and the calcium atoms. In short, this simulation was accomplished by solvating the protein in a 40 Å box of water. Initially, the H_2O, Ca^{2+} and Na^+ (counterion for charge neutralization) were energy minimized at constant volume as previously described (*46*). Since the NMR constraints had determined the backbone conformation a Particle Mesh Ewald molecular dynamics simulation was performed on the side chains of the calcium coordinating residues and on the Ca^{2+}, Na^+ and water molecules only for 350 ps at constant pressure and with fixed backbone.

RESULTS

A solution of bovine osteocalcin was titrated with Ca^{2+} and 1D ^{1}H NMR spectra were collected to determine the amount of Ca^{2+} needed to induce the maximum conformational change. Figure 1 shows a few sample spectra from the ^{1}H 1D NMR titration of bovine osteocalcin (1.0 mM) with Ca^{2+} in the presence of 20 mM NaCl. Significant shifts in both aliphatic and aromatic protein resonances are observed with Ca^{2+} addition. We found no additional spectral changes above 3 mM Ca^{2+} (Figure 1), which indicates a stoichiometry of Ca^{2+}/Ost of 3 is needed for the conformational change. This result is in agreement with previous calcium binding studies (*49*, *50*) and was also corroborated by CD titrations, when under the same solution conditions the maximum conformational change was complete by 3 mM $CaCl_2$. The data used to determine the three-dimensional structure of Ca^{2+}-osteocalcin in this study were collected from a solution containing 1.65 mM protein, 20 mM NaCl, and 6 mM $CaCl_2$ to ensure that there was sufficient $CaCl_2$ present to induce the maximum conformational change. Additional NaCl did not change the amount of α-helix predicted by circular dichroism nor did it change the appearance of the 1D ^{1}H NMR spectrum of apo- or Ca^{2+}-osteocalcin.

In agreement with previous circular dichroism studies on bovine osteocalcin (*20*−*22*), a lack of structure for the apo-protein is suggested by the NMR data as well. Inspection of Figure 1 shows calcium addition causes shifts in resonances from carboxylic acid containing amino acid residues such as the β protons of Gla and Glu (2.2 ppm) and of Asp and Asn (2.5−3.0 ppm), as well as the γH proton of Gla (3.0−3.3 ppm) as compared to those in the apo protein. Significant shifts were also observed in resonances from side chain protons of hydrophobic residues such as Val γCH_3, Leu

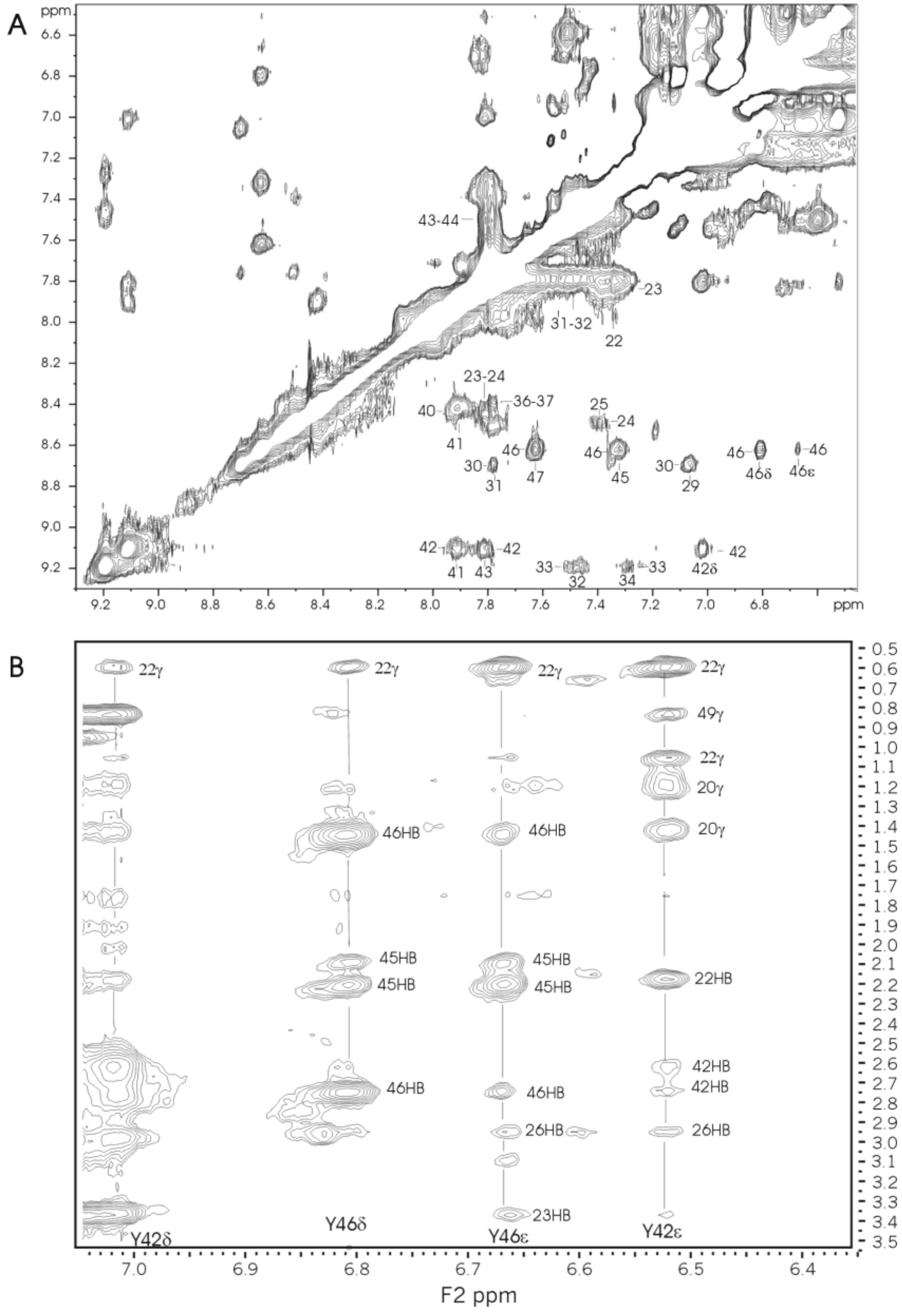

FIGURE 2: The two-dimensional ^{1}H NMR spectra of (A) the amide−amide proton region and (B) the aromatic−aliphatic proton region of the NOESY spectrum collected in H_2O at 37 °C with a 150 ms mixing time. The sequential amide protons are labeled by residue number in panel A. Long-range contacts involving aromatic side chain protons are labeled in panel B.

δCH_3, and Ile γCH_2 (1.1 ppm), as well as in resonances from the aromatic side chains of Tyr and Phe (6.6−7.1 ppm). This suggests that Ca^{2+} induces a conformational change in the protein and that it may induce hydrophobic interactions within the molecule. We were not able to obtain cross-peaks in a 2D ^{1}H NOESY spectrum of apo osteocalcin, so it is not possible to solve the structure. However, all available data from CD and NMR suggest a rather extended, unstructured conformation.

All proton resonances were sequentially assigned using a combination of two-dimensional DQF-COSY, short- and long-mix TOCSY, and NOESY experiments. NOESY experiments in ^2H_2O were used to identify interactions between aromatic side chains and aliphatic protons. Sequential assignments were made using the NH-αH region as well as the amide-amide region of the NOESY spectra. The amide–amide region of the NOESY spectrum in H_2O is shown in Figure 2a. Stronger sequential amide proton contacts are indicative of α-helical structure. Some of the connectivities between the amide protons of residues 22–46 are shown, with some amide signals being obscured by the diagonal. Long-range contacts were also observed in the NOESY spectrum. Figure 2b show NOEs between the aromatic side chain of Y46 with side chain protons of N26, C23, and V22. Similar long-range interactions are also observed between the aromatic side chain of Y42 with side chain protons of N26, C23, V22, and R20. The shifted methyl protons in the 1D spectrum are due to the interaction with these aromatic side chains.

Structural Constraints. The structure of Ca^{2+}-osteocalcin was derived from 448 NOE distance constraints, 94 of which were intraresidue, 171 were sequential, 125 were medium range, and 58 were long range. There were also 34 dihedral constraints, 41 χ angle constraints, 45 H_α, 36 C_α, and 39 C_β chemical shifts used in the calculation. Figure 3 shows the distribution of NOE distance constraints along the sequence of osteocalcin. It can be seen that the medium range and longer range NOEs are predominantly located within the region of residues 16–49. The decreased number of medium range and the lack of longer range NOEs in the region of residues 1–15 are indicative of a lack of structure. The backbone NOE patterns are shown in the lower half of Figure 3. Intense NH–NH NOEs are characteristic of an α-helix and are predominantly observed from residues 22–47. Since proline does not have an NH proton no NH–NH NOEs are expected in those regions. Other weaker proton NOE patterns between nonsequential residues ($d_{\alpha N}$ $(i,i+3)$, $d_{\alpha\beta}(i,i+3)$, $d_{\alpha N}$-$(i,i+4)$, and $d_{NN}(i,i+2)$) are also indicative of the presence of helical structure. As can be seen in Figure 3, some of these patterns are observed within residues 19–26, 27–34, and 44–47. Secondary proton chemical shifts are also shown in Figure 3. These values represent the difference between the observed αH chemical shift from that reported in a random coil conformation. A group of residues exhibiting positive secondary shifts of 0.15–0.6 ppm is indicative of a helical conformation, with reduced values indicating greater flexibility (*51*). Positive values for ^{13}C secondary shifts are also observed in areas of α-helical structure (*51*). Examination of the lower half of Figure 3 shows elevated ^{1}H and^{13}C secondary shift values for similar regions showing intense NH–NH NOES, namely, residues 20–24, 29–33, and 42–45. The majority of the measured temperature coefficients gave values of less than 5 for NH protons in residues 14–38 and 41–47, indicating folded regions in the molecule and the probability that these protons are hydrogen bonded. The calculated structures were consistent with nine hydrogen bonds. The NH protons involved in hydrogen bonds are marked in Figure 3 with circles. Overall the data indicates 3 structured areas in the molecule, namely residues 20–25, 29–34, and 42–46. The lack of long-range NOEs, NOE structural patterns, hydrogen bonds, and elevated ^{1}H and ^{13}C secondary shifts in residues 1–15 indicate the N terminus to be an unstructured region of the molecule.

Structure Calculation and Description. The structures were calculated using torsion angle dynamics and refined using

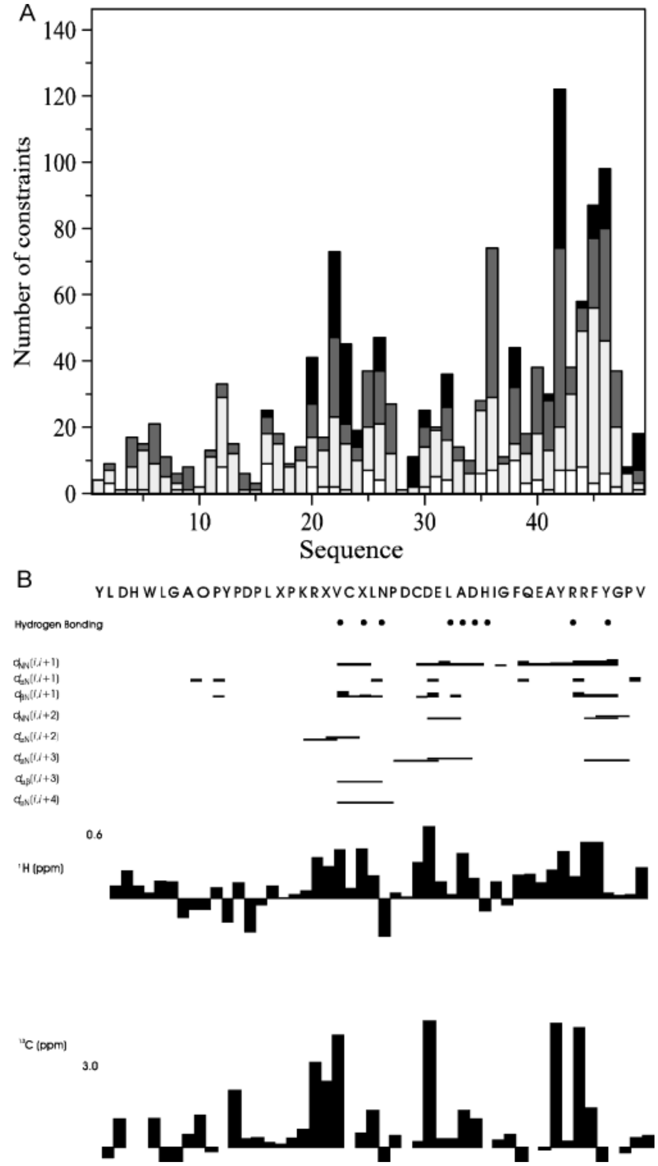

FIGURE 3: NOE constraints per residue are shown in panel A, where black bars indicate long-range NOES, dark gray bars indicate medium range NOES, light gray bars indicate sequential NOES, and white bars indicate intrarresidue NOES. A summary of NMR restraints for Ca^{2+}-osteocalcin is shown in panel B. The black circles indicate hydrogen bonds derived from multiple temperature experiments. The horizontal lines indicate backbone NOES with the thickness representing intensity. The H_α and $^{13}C_\alpha$ chemical shift deviations from random coil values are also shown.

simulated annealing and energy minimization using the program CNS (*43*). The N terminus did not have many constraints, was highly flexible and unstructured, and could not be confined to any fixed orientation with respect to the rest of the molecule. The 13 lowest-energy structures showing the structured region (residues 16–49) are shown in the bundle in Figure 4a. The total backbone rmsd for this region is 1.09 Å, and there were no distance restraint violations greater than 0.3 Å and no dihedral angle restraint violations greater than 5°. This indicates that the structures fit the NMR data well and that one conformation can be defined for the molecule. The three structured regions, shown in Figure 4b–d, have a backbone rmsd of 0.67 (residues 17–25), 0.67 (residues 27–35), and 0.14 Å (residues 41–45). Superposition of the Gla region with the side chains in

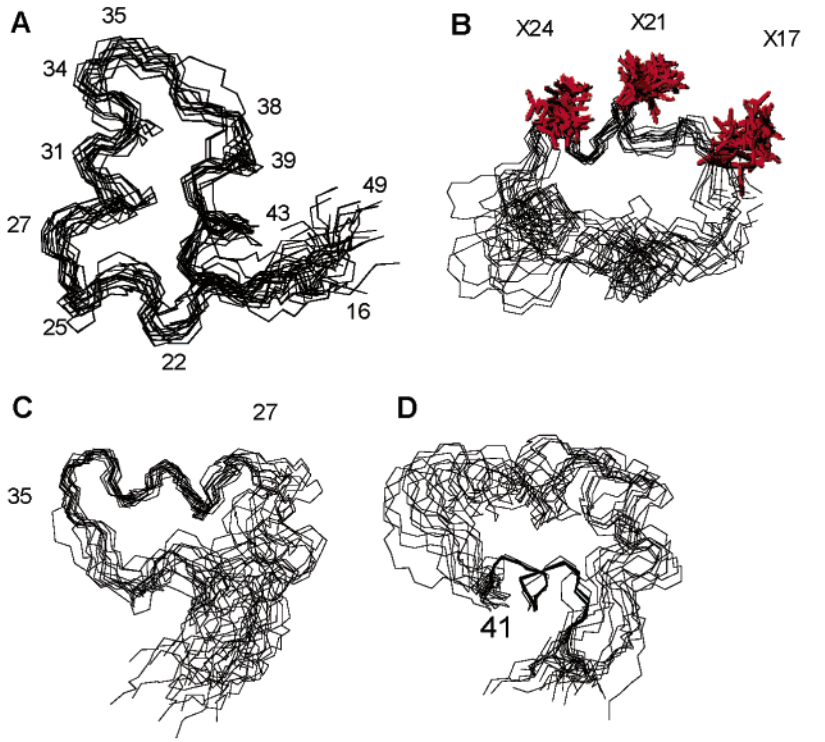

FIGURE 4: The structured region (residues 16−49) of the 13 best conformers of Ca^{2+}-osteocalcin. Superposition of the backbone atoms for residues 16−49 is shown in panel A, 17−25 is shown in panel B, 27−35 is shown in panel C, and 41−45 is shown in panel D. The RMSD's for the various regions are given in the Structural Statistics in Table 1.

Table 1: Structural Statistics

total number of NOE constraints	448
intraresidue	94
sequential	171
medium range	125
long range	58
largest distance constraint violation (Å)	0.30
RMSD	
backbone (Å)	1.09 (residues 16−48)
	0.67 (residues 17−25)
	0.67 (residues 27−35)
	0.14 (residues 41−45)
heavy atoms (Å)	1.5 (residues 17−25)
deviations from idealized geometry	
1.5 (residues 17−25) bonds (Å)	0.00319
1.5 (residues 17−25) angles (deg)	0.4325
van der Waals energy (kcal/mol)	−206.6
Ramachandran plot	67.7% most favorable region
	32.3% in additionally and generously allowed

residues 17−25 gives an rmsd of 1.51 Å. The structural statistics are shown in Table 1.

The lowest-energy structure of Ca^{2+}-osteocalcin is shown in Figure 5A. As can be seen in the figure there is an unstructured N terminus from residues 1−15 and a structured region from residues 16−49 which contains three regions of secondary structure. Since the N-terminal region could not be confined to a fixed orientation with respect to the rest of the molecule, it is oriented differently in each model within the family of structures. The N-terminal region also did not contain any areas of secondary structure although interactions between the hydrophobic side chains of Leu2 and Trp5 were observed. Analysis of ϕ and θ backbone torsion angles allow classification of the areas of secondary structure within the structured region (*16*−*49*). Residues 20−26 have quasihelical structure with residues 20−23 and 23−26 forming two type III near reverse turns (*52*). Residues 27−35 had α-helical characteristics for most of the structures although some of the structures were classified as a 3_{10} helix in this region. A disulfide bond between Cys23 and Cys29 separates the first and second helical regions. The helical segment from residues 41−44 was classified as an α-helix for all models. Hydrogen bonds within these three regions serve to stabilize the helical structures. The tertiary structure of the molecule consists of a C-terminal core (residues 16−49) formed by various long range and hydrophobic side chain interactions such as those between Leu 16 and Phe 45, and between Tyr 42 and Tyr 46, with Val 22 and Cys 23 as shown in Figure 5B. These long-range hydrophobic interactions also serve to stabilize the type III turns within residues 20−26.

Docking of Ca^{2+} in Osteocalcin. The NMR titration data as well as previous studies have indicated that 3 mol of Ca^{2+} are bound per mole of bovine osteocalcin, and the NMR titration data show that 3 mol of calcium per mole of osteocalcin is responsible for the conformational change. The genetic algorithm−molecular dynamics simulation method, applied to other NMR structures of Ca^{2+} binding Gla containing peptides and proteins (*46*, *53*), was used to identify the positions of the calcium ions. All 13 conformers in the family of structures were searched with the genetic algorithm and the most frequently occurring coordinated structure had each of the three Gla residues coordinating a calcium ion. The orientation of the N-terminal unstructured region of the protein cannot be defined and is in a different position in each conformer. The N-terminal region had no sole coordination site and was predominantly uncoordinated in all 13 conformers. Thus, an average structure was created from residues 16−49, and the genetic algorithm identified calcium ion positions that gave the lowest-energy structure.

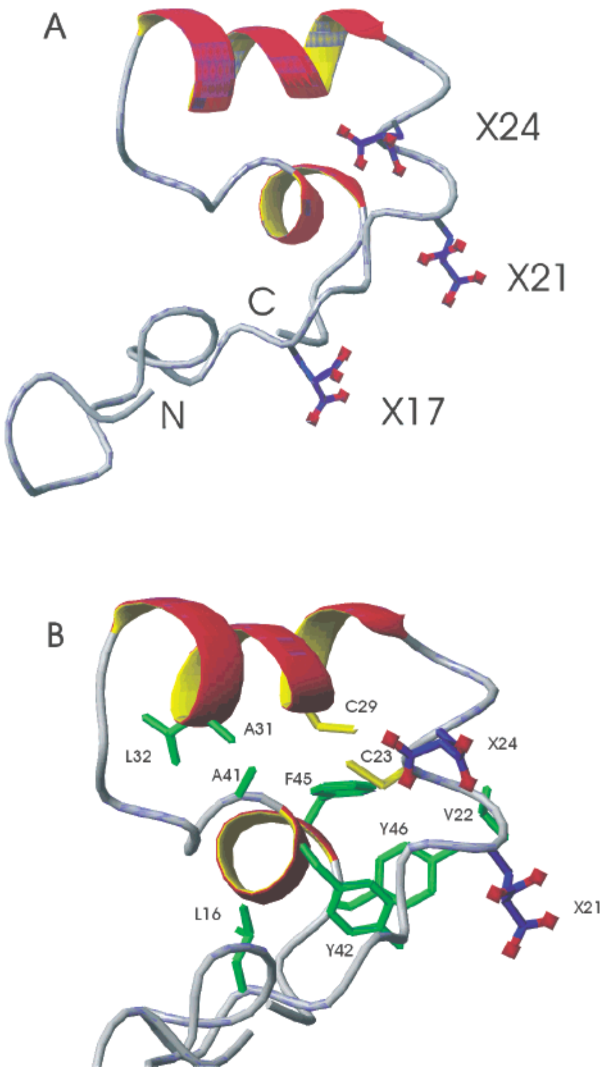

FIGURE 5: The ribbon diagram of the lowest-energy conformer of Ca^{2+}-osteocalcin is shown in Figure A. The N-terminal region (residues 1−15) is unstructured and cannot be confined to a fixed orientation with respect to the rest of the molecule. There is a core in the C-terminal region (residues 16−49), which has helical content. The three Gla residues (×17, ×21, ×24) are surface exposed. Some of the hydrophobic side chains within the core of the molecule are shown in panel B. Long-range interactions were observed between the aromatic and aliphatic side chains of F45 and L16 as well as Y46, Y42 and V22, and C23 and C29.

This structure, along with one Na^+ atom to balance the charge, was solvated in water and subjected to a molecular dynamics simulation where the Gla side chains and the ions have their geometries and energy optimized. This procedure resulted in a coordination pattern where the three calcium atoms were mainly coordinated to the three Gla residues as shown in Figure 6A. A calcium atom was considered to be coordinated to an oxygen atom if the distance between the two atoms was less than 3 Å. One calcium atom was coordinated by the side chain oxygen atoms OD1 and OD2 of Asp30, the side chain oxygen atom OE1 of one of the carboxyl groups of Gla24, and the oxygen atoms of three water molecules. The second calcium atom was coordinated to two of the oxygen atoms, OE3 and OE4 of the second carboxyl group of the side chain in Gla 24, to two oxygen atoms OE1 and OE2 of one of the carboxyl groups of Gla 21, and to the oxygen atoms of two water molecules. The third calcium atom was coordinated to the oxygen atoms of

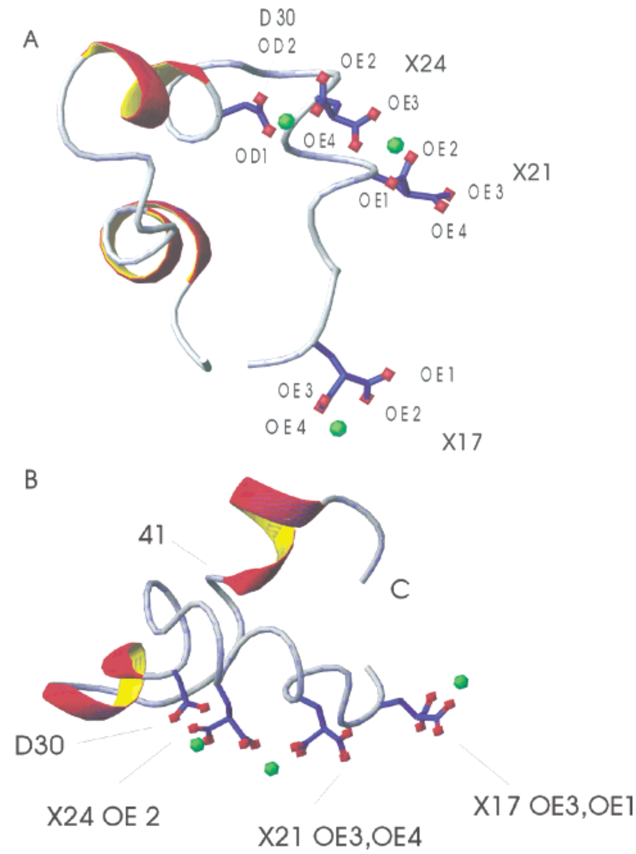

FIGURE 6: (A and B) The final calcium coordinated structure of osteocalcin (residues 16−49) after molecular dynamics simulation is shown in panels A and B where the calcium atoms are shown in green. A genetic algorithm determined calcium placement, and the structure was then subjected to a molecular dynamics simulation as described in Materials and Methods. Figure B shows the calcium-bound structure in the bone binding orientation where the free, uncoordinated oxygen atoms on the Gla (X) residues are clearly labeled.

each carboxyl group of Gla17, OE2, and OE4 as well as to the oxygen atoms of three water molecules.

Ultracentrifugation Measurements of Ca^{2+}-Osteocalcin. Sedimentation equilibrium experiments were conducted to determine the oligomerization state of Ca^{2+}-osteocalcin. The best fit to the data gave a molecular weight of 8212 ± 363, which is appreciably greater than the calculated monomer molecular weight of 5850. This result clearly indicates some self-association of the protein. Fitting of these data to a monomer−dimer association model yields a dimerization constant of 6258 ± 1600 M^{-1} (K_d = 160 μM), indicating that 80% of the protein is dimeric at the 1.65 mM protein concentrations used in this study. Only one set of cross-peaks was observed in all 2D NMR spectra, indicating that all protein molecules have the same conformation. No aberrant or inconsistent NOE cross-peaks were observed, and all NOE cross-peaks were used in the structure calculation with no distance constraint violations over 0.3 Å. This suggests that all observed NOEs were intramolecular rather than intermolecular at the dimer interface. A number of long range NOE interactions (Y42, Y46, and V22, etc.) were observed which could potentially be intermolecular NOES at a dimer interface rather than intramolecular NOES. To test this possibility, we omitted these long-range NOES from the structure calculation and obtained the same general backbone fold and same secondary structural characteristics with the exception of the close proximity of those hydrophobic side chains responsible for the observed NOEs. Also, the identical 1D NMR spectrum with the shifted resonances from Tyr and Val is observed both at 50 μM protein (70% monomer) and at 1.65 mM protein (20% monomer, 80% dimer). This suggests that the same hydrophobic interactions occur in the monomer and are intramolecular. Finally, CD spectra collected at protein concentrations where the protein is predominantly monomeric (50 μM) indicated that approximately 20% percent of the protein is in an α-helical conformation (*23*). This finding is in agreement with that determined from the structure in the present study (24% α-helical) at concentrations where the dimer predominates. Preliminary sedimentation equilibrium studies gave a weight average molecular weight for apo-osteocalcin of 6289 ± 104, suggesting that it is 90−95% monomeric under these experimental conditions. The difference between the weight average molecular weight values of apo- and Ca^{2+}-bound osteocalcin suggests a calcium binding mediated self-association. The data point to a symmetric dimer where the structure that was solved is of the individual monomers. Our data cannot determine the location of the dimer interface, but since it is a metal induced dimerization, it may be at the calcium binding sites. In vivo the concentration of circulating osteocalcin is in the nanomolar range, which would indicate it is all monomeric. Most of the osteocalcin is bound to bone mineral and accumulates with time so that it is difficult to estimate the local concentration at the bone surface at any given time. Most likely, after it is secreted from the osteoblast, it is mineral bound and in the monomeric form.

DISCUSSION

In this paper we have solved the first high-resolution structure of a noncollagenous bone protein. Our study is in general agreement with the pieces of structural information on osteocalcin reported previously. Data obtained from CD and 1D NMR studies showed that Ca^{2+}-induced an α-helical conformation in 15−34% of the protein and shifted aromatic and aliphatic side chain resonances (*21*−*23*, *54*). Fluorescence, ultraviolet CD, and UV absorption studies showed an alteration in the environment of tyrosine and phenylalanine residues, suggesting decreased exposure to polar solvent (*19*). As shown in Figure 5B, both tyrosine and phenylalanine residues are located within the hydrophobic core of the molecule and are involved in longer range hydrophobic interactions. The structure is consistent with these data since these residues are indeed more buried and less solvent exposed. A previous 2D NMR study using a lower field spectrometer (500 MHz) was unable to define a single conformation for rabbit Ca^{2+}-osteocalcin (*55*). However, long-range interactions between side chains of hydrophobic residues were reported which is in agreement with the observations in this study. The higher field and, perhaps, better optimization of solution conditions allowed for the detection of a greater number of NOE distance constraints, increasing the likelihood that a single conformation will be defined. The 133 NOE distance constraints detected in the previous study versus 448 detected in the present study attest to this.

The genetic algorithm−molecular dynamics approach was used to predict the positions of the three calcium atoms in osteocalcin. This approach was chosen because it was found to correctly identify the 7 calcium ion positions in the crystal structure bovine prothrombin factor 1 (*46*). It has since been used to identify calcium positions in other Gla containing structures such as coagulation factor IX (*46*) and in conatoxin peptides (*53*). Other approaches such as the use of paramagnetic probes (Ce^{3+}) have the disadvantage of possibly altering the structure from that which would be obtained in the calcium bound state. The advantage of using the genetic algorithm is that it is a theoretical approach and does not physically perturb the structure. This method predicted the placement of the three calcium atoms on the Gla residue carboxyl groups and to one Asp residue. This prediction is validated by experimental evidence. A mass spectrometry study showed that osteocalcin bound to three atoms of calcium was the major species and that calcium binding was lost upon decarboxylation of the Gla residues to Glu (*49*). A ^{45}Ca equilibrium dialysis study also indicated that a minimum of three calcium atoms are bound per mole of bovine osteocalcin (*49*). In addition, a loss of calcium binding to bovine osteocalcin was shown with decarboxylation of Gla to Glu (*6*). It has also been shown by CD that Gla 17 is needed for the calcium induced α-helical structural change suggesting it is also coordinated (*20*).

Bovine osteocalcin has a unique fold as compared to other calcium binding proteins as well as Gla containing blood coagulation factors. In contrast to other calcium binding proteins (i.e., calmodulin, Factors IX and X) (*56*, *57*, *1*), apo-osteocalcin is relatively unstructured except for a disulfide bond between Cys23 and Cys29. Calcium addition induces a folded structure containing several helical regions, a C-terminal hydrophobic core, and an unstructured N-terminus. The Gla residues which coordinate calcium are on the same face of the helical region and are surface exposed. In contrast, with calcium addition, the complexes of factor IX (*2*), prothrombin (*3*), and that proposed for factor X (*1*) have the calcium coordinated Gla residues reoriented inward, most of which are not surface exposed. However, similar longer-range interactions or proximity between aromatic and methyl side chain protons and aromatic side chains and disulfide loops are observed in Factor IX and prothrombin as well (*2*, *3*). The global fold of Factor IX (residues 1−47), similar to that in prothrombin, consists of an amino terminal loop adjacent to a large carboxy terminal core. Although osteocalcin also has a carboxy terminal core, it differs from the coagulation proteins in that the amino terminus is unstructured and flexible.

The structure for Ca^{2+}-osteocalcin reported in this study is different from the model predicted previously (*19*). The model predicted two antiparallel α-helical domains, the Gla-containing helix (residues 18−25) and the Asp−Glu-containing helix (residues 30−41) connected by a β-turn formed by residues 26−29 and stabilized by a Cys_{23}−Cys_{29} disulfide bond. A second β-turn was predicted at residues 12−15 and 6−7 residues at both the N and C termini were predicted to be in a β-sheet structure and in close proximity (*19*). The tertiary structure we report is different because hydrophobic side chains in the C terminal region interact with those in the middle portion of the molecule forming a loop from residues 16−49 so that the N and C termini are not involved in a β-sheet conformation. Since the orientation of the N terminus is not constrained with respect to the rest of the molecule, it may or may not be close to the C terminus.

Also, there is no β-turn within residues 26−29 so that the two helical regions are not antiparallel. In addition, the majority of the structures do not show a turn within residues 12−15. However, our structure is in reasonable agreement with some of the secondary structural elements predicted by the model, and the three Gla residues do project from the same face of the helical region.

The structure is consistent with many reported properties of osteocalcin. The C-terminal pentapeptide FYGPV and an octapeptide were found to have chemotactic activity to osteoclast precursor cells (*11*, *58*). Previous studies have shown that plasmin, which is associated with osteoblast membranes, cleaves osteocalcin at the C-terminal between residues 43 and 44, arg−arg (or lys−arg), producing two peptides comprising residues 1−43 and 44−49 (*59*). Figure (*6*B) shows the osteocalcin structure in the bone binding orientation, and it is clear that the C-terminus extends outward and would be accessible to neighboring cells as well as endogenous proteinases. A study showing that the serine proteases, cathepsin D, L, and H degrades osteocalcin at the 7−8 bond is consistent with an unstructured N-terminus (*60*).

It has been proposed that the distance between the free uncoordinated oxygen atoms of the Gla carboxyl groups of Ca^{2+}-osteocalcin can interact with intercalcium spacings of 5.4 Å in the hydroxyapatite lattice (*19*). Evidence for involvement of the Gla residues with crystal binding comes from the demonstration that hydroxyapatite binding prevents Gla decarboxylation (*6*). From reported X-ray data, the calculated spacings between calcium atoms in hydroxyapatite are 3.44, 4.06, 5.45, 5.84, 6.33, 6.88, and 9.43 Å (*19*, *24*). The spacings between the free oxygen atoms of the Gla carboxyl groups can be measured from the Ca^{2+}-coordinated structure of osteocalcin. In our study, the distances were measured from the best final structure, and the errors were calculated from averaging these positions in all structures in the molecular dynamics simulation, taking into account the flexibility in the side chains of the Gla residues. The χ side chain angles are more constrained in Gla24 and Gla 21 because the calcium is coordinated between two residues, whereas those in Gla 17 are more flexible since this residue alone coordinates a calcium atom. The free oxygen atoms of the Gla carboxyl groups are OE2 of Gla 24, OE3 and OE4 of Gla 21, and OE3 and OE1 of Gla 17 as shown in Figure 6B. The spacing between OE2 of Gla 24 and OE3 of Gla21 is 9.96 ± 0.90 Å, between OE2 of Gla24 and OE4 of Gla21 is 10.2 ± 0.90 Å, between OE4 of Gla21 and OE1 of Gla17 is 11.0 ± 2.5 Å, and between OE3 of Gla21 and OE1 of Gla17 is 10.0 ± 2.50 Å. The range in the calculated distances of the Gla side chains indicates that the best correlation is with the intercalcium distance of 9.43 Å, rather than the 5.44 Å as previously suggested (*19*). The unit cell dimensions of the hydroxyapatite crystal are $a = b = 9.43$ Å and $c = 6.88$ Å (*24*). The intercalcium distance of 9.43 Å is located between calcium atoms within the *ac* and *ab* faces of the unit cell of hydroxyapatite crystals (*24*). Figure 7A shows how the uncoordinated oxygen atoms of the Gla carboxyl groups can interact with the calcium atoms in hydroxyapatite. It also shows that two of the coordinated calcium atoms on the Gla residues are aligned with calcium atoms in the mineral. This indicates that the calcium atoms coordinated to the protein can also fill in vacant positions in the crystal lattice, as was also proposed (*19*). Both proposed

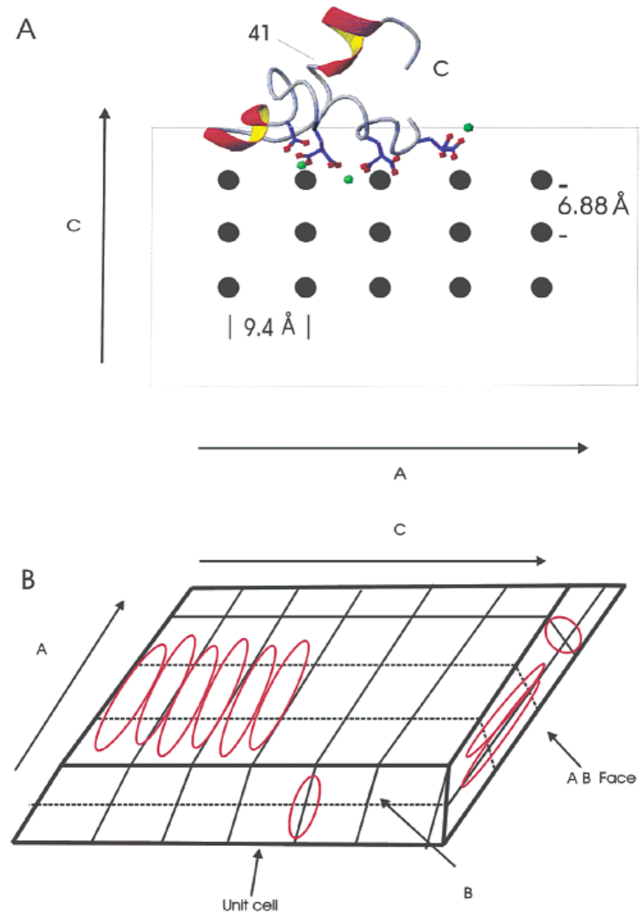

FIGURE 7: The proposed mechanism for calcium coordinated osteocalcin interacting with bone mineral. The free oxygen atoms of the Gla residues labeled in Figure 6B can bind to calcium atoms in the mineral spaced at 9.4 Å apart as shown in panel A. The accessible C terminus in the bone binding orientation is labeled. An illustration of a bone mineralite composed of unit cells is shown in panel B. Examples of binding sites for osteocalcin where calcium atoms are separated by 9.4 Å in the mineral are shown in red ellipses.

mechanisms for Ca^{2+}-osteocalcin binding to bone may be operative. A recent study using atomic force microscopy in bone found that mineralites are 20 Å thick or less and have a platelike shape. The long axis is parallel to the unit cell *c* axis in hydroxyaptite and is approximately 117 Å long, and the width is approximately 103 Å wide (*61*). This would indicate that the intercalcium sites in bone which are most complimentary for the Gla side chains in osteocalcin are located on the most exposed ac face of the crystal and also at the crystal ends on the ab face. Some possible binding sites on the bone mineralite are shown in Figure 7B.

The structure and proposed mechanism for the binding of osteocalcin to hydroxyapatite may help explain results obtained from previous binding studies. We have reported that the presence of millimolar amounts of calcium induced a significant increase of 40% in the occupancy of binding sites on the crystal as compared to the metal free apo-protein (*22*). The structure reported in this study shows that calcium induces a more compact structure in the molecule as compared to the unstructured apo-protein resulting in enhanced occupancy of binding sites on the crystal. A more compact structure in the presence of calcium as compared to the apo-protein was also observed in gel filtration studies of dog osteocalcin (*54*). Another study using fluorescently labeled protein reported that there was preferential adsorption of osteocalcin to the [100] face (equivalent to *ac* or *bc* face in hexagonal crystals) as compared to the [001] (*ab*) face (*62*). As shown in Figure 7b, the rows of calcium with compatible intercalcium spacings of 9.43 are located every 6.88 and 3.44 Å in the *ac* face and are parallel to each other. On the [001] or *ab* face of the crystal, these calcium rows are perpendicular to each other such that protein binding to one site prevents binding to another due to overlap. The increased availability of binding sites may explain the preferential binding of osteocalcin to the ac face.

Despite the considerable advancement in our understanding of the biology of osteocalcin, the function of osteocalcin has not been precisely defined. Studies have suggested that osteocalcin, by virtue of its high concentration in bone, functions within the bone matrix and can directly affect bone cells (*63*). Intact osteocalcin and a COOH terminal octapeptide were shown to be chemoattractants for human peripheral blood monocytes (*58*), and subcutaneous implantation of osteocalcin deficient bone showed a decrease in the number of differentiated multinucleated osteoclast like cells surrounding the bone particles (*15*). However, none of these potential functions have been unequivocally proven. Although the osteocalcin null mouse has no defect in osteoclast activity (*16*), detailed examination of bone mineral properties did reveal a decrease in crystal size suggesting a role in bone remodeling (*17*).

It is also possible that the soluble protein may be the important component of osteocalcin's function and its Gla residues may serve as a means to affix it onto the mineralized surface, thereby maintaining an equilibrium between soluble and mineral bound protein. Changes in that equilibrium due to vitamin K deficiency may be an important regulator of any role osteocalcin plays in skeletal dynamics, be it in the soluble form or bound to bone. In humans, associations among low bone mass, increased risk of hip fracture, and low vitamin K intake have been observed.

In summary we have provided detailed, high-resolution structural information on a noncollagenous bone protein which heretofore had not been examined. We have proposed a mechanism for mineral binding via uncoordinated oxygen atoms from its three Gla side chain COOH groups. This model may shed light on the mechanism of impaired mineral binding seen in undercarboxylated forms of osteocalcin or observed in the presence of other metals such as Mg^{2+}. This structural information will hopefully provide insight or support to some of the reported biological properties and aid in further defining the function of this protein.

ACKNOWLEDGMENT

The authors are especially thankful to Dr. Mark Girvin for expert advice and helpful discussions. The authors would also like to thank Dr.'s S. Cahill, S. Englard, S. Almo, and R. Gupta for helpful discussions. The authors are grateful to Dr. R. Angeletti, Dr. L. Mints, and E. Nieves in the Laboratory for Macromolecular Analysis and Proteomics for expertise in the synthesis and characterization of the protein.

SUPPORTING INFORMATION AVAILABLE

Table of NMR assignments. This material is available free of charge via the Internet at http://pubs.acs.org.

REFERENCES

1. Sunnerhagen, M., Forsen, S., Hoffren, A., Drakenberg, T., Teleman, O., and Stenflo, J. (1995) *Nat. Struct. Biol. 2*, 504−509.
2. Freedman, S. J., Furie, B. C., Furie, B., and Baleja, J. D. (1995) *Biochemistry 34*, 12126−12137.
3. Soriano-Garcia, M., Padmanabhan, K., de Vos, A. M., and Tulinsky, A. (1992) *Biochemistry 31*, 2554−2566.
4. Hauschka, P. V., Lian, J. B., and Gallop, P. M. (1975) *Proc. Natl. Acad. Sci. U.S.A. 72*, 3925−3929.
5. Price, P. A., Otsuka, A. S., Poser, J. W., Kristaponis, J., and Raman, N. (1976) *Proc. Natl. Acad. Sci. U.S.A. 73*, 1447−1451.
6. Poser, J. W., and Price, P. A. (1979) *J. Biol. Chem. 254*, 431−436.
7. Price, P. A., Otsuka, A. S., Poser, J. W., Kristaponis, J., and Raman, N. (1976) *Proc. Natl. Acad. Sci. U.S.A. 73*, 1447−1451.
8. Romberg, R. W., Werness, P. G., Riggs B. L., and Mann, K. G. (1986) *Biochemistry 25*, 1176−1180.
9. Boskey, A. L., Wians, F. H., and Hauschka, P. V. (1985) *Calcif. Tissue Int. 37*, 57−62.
10. Hunter, G. K., Hauschka, P. V., Poole, A. R., Rosenberg, L. C., and Goldberg, H. A. (1996) *Biochem. J. 317*, 59−64.
11. Mundy, G. R., and Poser, J. W. (1983) *Calcif. Tissue Int. 35*, 164−168.
12. Malone, J. D., Teitelbaum, S. L., Griffin, G. L., Senior, R. M., and Kahn, A. J. (1982) *J. Cell. Biol. 92*, 227−235.
13. Lian, J. B., Dunn, K., and Key, L. L. (1986) *Endocrinology 118*, 1636−1642.
14. Glowacki, J., Rey, C. Glimcher, M. J., Cox, K. A., and Lian, J. (1991) *J. Cell. Biochem. 45*, 292−302.
15. DeFranco, D. J., Glowacki, J., Cox, K. A., and Lian, J. B. (1991) *Calcif. Tissue Intl. 49*, pp. 43−50.
16. Ducy, P., Desbois, C., Boyce, B., Pinero, G., Story, B., Dunstat, C., Smith, E., Bonadio, J., Goldstein, S., Gundberg, C., Bradley, A., and Karsenty, G. (1996) *Nature 382*, 448−452.
17. Boskey, A., Gadaleta, S., Gundberg, C., Doty, S. B., Ducy, P., and Karsenty, G. (1998) *Bone 23*, 187−196.
18. Hauschka, P. V., Lian, J. B., Cole, D. E. C., and Gundberg, C. M. (1989) *Physiol. Rev. 69*, 990−1047.
19. Hauschka, P. V., and Carr, S. A. (1982) *Biochemistry 21*, 2538−2547.
20. Nakao, M., Nishiuchi, Y., Nakata, M., Kimura, T., and Sakakibara, S. (1994) *Peptide Res. 7*, 171−174.
21. Gundlach, G., and Voegeli, R. (1983) *Hoppe-Seyler's Z. Physiol. Chem. Board 364*, 31−39.
22. Dowd, T. L., Rosen, J. F., Mints, L., and Gundberg, C. M. (2001) *Bioch. Biophys. Acta 1535*, 153−163.
23. Delmas, P. D., Stenner, D. D., Romberg, R. W., Riggs, B. L., and Mann, K. G. (1984) *Biochemistry 23*, 4720−4725.
24. Kay, M. I., Young, R. A., and Posner, A. S. (1964) *Nature 204*, 1050−1052.
25. Babu, Y. S., Bugg, C. E., and Cook, W. J. (1988) *J. Mol. Biol. 204*, 191−204.
26. Barbato, G., Ikura, M., Kay, L. E., Pastor, R. W., and Bax, A. (1992) *Biochemistry 31*, 5269−78.
27. Herzberg, O., and James, M. N. G. (1985) *Nature 313*, 653−659.
28. Gagné, S. M., Tsuda, S., Li, M. X., Smillie, L. B., and Sykes, B. D. (1995) *Nature Struct. Biol. 2*, 784−789.
29. Skelton, N. J., Kördel, J., Akke, M., Forsen, S., and Chazin, W. J. (1994) *Nature Struct. Biol. 1*, 239−245.
30. Gundberg, C. M., Hauschka, P. V., Lian, J. B., and Gallop, P. M. (1984) *Methods Enzymol. 107*, 516−544.
31. Merrifield, B. (1997) *Methods Enzymol. 289*, 3−13.
32. Annis, I., Hargittai, B., and Barany, G. (1997) *Methods Enzymol. 289*, 198−220.
33. Philo, J. S. (1997). *Biophys J. 72*(1), 435−44.
34. Hwang, T. L., and Shaka, A. J. (1998) *J. Magn. Reson. 135*, 280−287.
35. Marion, D., and Wüthrich, K. (1983) *Biochem. Biophys. Res. Commun. 113*, 967−974.
36. Marion, D., Ikura, M., Tschudin, R., and Bax, A. (1989) *J. Magn. Reson. 85*, 393.
37. Delaglio, F., Grzesiek, S., Vuister, G. W., Zhu, G., Pfeifer, J., and Bax, A (1995) *J. Biomol. NMR. 6*, 277−293.
38. Johnson, B. A., and Blevins, R. A. (1994) *J. Biol. Phys. 29*, 1012−1014.
39. Wüthrich, K. (1986) in *NMR of Proteins and Nucleic Acids* (Wiley Ed.) John Wiley and Sons, New York.

40. Bax, A., and Davis, D. G. (1985) *J. Magn. Reson. 65*, 355−360.
41. Cornilescu, G., Delaglio, F., and Bax, A. (1999) *J. Biomol. NMR 13*, 289−302.
42. Güntert, P., Mumenthaler, C., and Wüthrich, K. (1997). *J. Mol. Biol. 273*, 283−298.
43. Brunger, A. T., Adams, P. D., Clore, G. M., DeLano, W. L., Gros, P., Grosse-Kunstleve, R. W., Jiang, J., Kuszewski, J., Nilges, M., Pannu, N. S., Read, R. J., Rice, L. M., Simonson, T., and Warren, G. L. (1998) *Crystallogr. NMR Syst.*: *Acta Crystallogr. D54*, 905−921.
44. Koradi, R., Billeter, M., and Wüthrich, K. (1996) *J. Mol. Graphics 14*, 51−55.
45. Laskowski, R. A., Rullmann, J. A. C., MacArthur, M. W., Kaptein, R., and Thornton, J. M. (1996) *J. Biomol. NMR 8*, 477.
46. Li, Leping, Darden, T. A., Freedman, S. J., Furie, B. C., Furie, B., Baleja, J. D., Smith, H., Hiskey, R. G., and Pedersen, L. G. (1997) *Biochemistry 36*, 2132−2138.
47. Pearlman, D. A., Case, D. A., Caldwell, J. A., Ross, W. S., Cheatman, T. E. I., Ferguson, D. M., Seibel, G. L., Singh, U. C., Weiner, P. K., and Kollman, P. A. (1995) *Amber*, Version 4.1, University of California, San Francisco.
48. Essmann, U., Perera, L., Berkowitz, M. L., Darden, T., Lee, H., and Pedersen, L. G. (1995) *J. Chem. Phys. 103*, 8577−8593.
49. Nousiainen, M., Derrick, P. J., Kaartinen, M. T., Maenpaa, P. H., Rouvinen, J., and Vainiotalo, P. (2002) *Chem. Biol. 9*, 195−202.
50. Price, P. A., Otsuka, A. S., and Poser, J. W. (1977) in *Calcium-Binding Proteins and Calcium Functions* (Wasserman, R. H., et. al., Eds.) pp 333−337, Elsevier/North-Holland, Amsterdam.
51. Wishart, D. S., Sykes, B. D., and Richards, F. M. (1991) *J. Mol. Biol. 222*, 311−333.
52. Crawford, J. L., Lipscomb, W. N., and Schellman, C. G. (1973) *Proc. Nat. Acad. Sci. U.S.A. 70*, 538−542.
53. Rigby, A. C., Baleja, J. D., Li, L., Pedersen, L. G., Furie, B. C., and Furie, B. (1997) *Biochemistry 36*, 15677−15684.
54. Isbell, D. T., Du, S. Schroering, A. G., Colombo, G., and Shelling J. G. (1993) *Biochemistry 32*, 11352−11362.
55. Atkinson, R. A., Evans, J. S., Hauschka, P. V., Levine, B. A., Meats, R., Triffitt, J. T., Virdi, A. S., and Williams, R. J. P. (1995) *Eur. J. Biochem. 232*, 515−521.
56. Kuboniwa, H., Tjandra, N., Grzesiek, S., Ren, H., Klee, C. B., and Bax, A. (1995) *Nature Struct. Biol 2*, 768−776.
57. Freedman, S. J., Furie, B. C., Furie, B., and Baleja, J. D. (1995) *J. Biol. Chem. 270*, 7980−7987.
58. Hauschka, P. V. (1985) Osteocalcin in its functional domains, in *The Chemistry and Biology of Mineralized Tissue* (Butler, W. T., Ed.) pp 149−158, Ebsco Media, Birmingham, AL.
59. Novak, J. F., Hayes, J. D., and Nishimoto S. K. (1997) *J. Bone Miner. Res. 12*, 1035−1042.
60. Baumgrass, R., Williamson, M. K., Price, P. A. (1997) *J. Bone Miner. Res. 12*, 447−455.
61. Eppell, S. J., Weidong, T., Katz, J. L., Kuhn, L., and Glimcher, M. J. (2001) *J. Orthopaed. Res. 19*, 1027−1034.
62. Fujisawa, R., and Kuboki, Y. (1991) *Biochim. Biophys. Acta 1075*, 56−60.
63. Bodine, P. V. N., and Komm, B. S. (1999) *Bone 5*, 535−543.

BI034470S